Matter and Radiation at Extremes

RESEARCH ARTICLE

pubs.aip.org/aip/mre

Induction heating for desorption of surface contamination for high-repetition laser-driven carbon-ion acceleration

Cite as: Matter Radiat. Extremes 8, 054002 (2023); doi: 10.1063/5.0153578
Submitted: 10 April 2023 • Accepted: 10 July 2023 •
Published Online: 28 July 2023

Sadaoki Kojima,[1,a)] Tatsuhiko Miyatake,[1,2] Hironao Sakaki,[1,2] Hiroyoshi Kuroki,[3] Yusuke Shimizu,[3] Hisanori Harada,[3] Norihiro Inoue,[3] Thanh Hung Dinh,[1] Masayasu Hata,[1] Noboru Hasegawa,[1] Michiaki Mori,[1] Masahiko Ishino,[1] Mamiko Nishiuchi,[1] Kotaro Kondo,[1] Masaharu Nishikino,[1] Masaki Kando,[1] Toshiyuki Shirai,[4] and Kiminori Kondo[1]

AFFILIATIONS

[1] Kansai Institute for Photon Science, National Institutes for Quantum Science and Technology (QST), 8-1-7 Umemidai, Kizugawa, Kyoto 619-0215, Japan
[2] Interdisciplinary Graduate School of Engineering Sciences, Kyushu University, 6-1, Kasuga-Koen, Kasuga, Fukuoka 816-8580, Japan
[3] Hitachi Zosen Corporation, 7-89 Nanko-Kita 1-chome, Suminoe-ku, Osaka 559-8559, Japan
[4] Department of Accelerator and Medical Physics, Institute for Radiological Science, National Institutes for Quantum Science and Technology (QST), 4-9-1 Anagawa, Inage-ku, Chiba 263-8555, Japan

[a)] **Author to whom correspondence should be addressed:** kojima.sadaoki@qst.go.jp

ABSTRACT

This study reports the first experimental demonstration of surface contamination cleaning from a high-repetition supply of thin-tape targets for laser-driven carbon-ion acceleration. The adsorption of contaminants containing protons, mainly water vapor and hydrocarbons, on the surface of materials exposed to low vacuum ($>10^{-3}$ Pa) suppresses carbon-ion acceleration. The newly developed contamination cleaner heats a 5-μm-thick nickel tape to over 400 °C in 100 ms by induction heating. In the future, this heating method could be scaled to laser-driven carbon-ion acceleration at rates beyond 10 Hz. The contaminant hydrogen is eliminated from the heated nickel surface, and a carbon source layer—derived from the contaminant carbon—is spontaneously formed by the catalytic effect of nickel. The species of ions accelerated from the nickel film heated to various temperatures have been observed experimentally. When the nickel film is heated beyond ~150 °C, the proton signal considerably decreases, with a remarkable increase in the number and energy of carbon ions. The Langmuir adsorption model adequately explains the temperature dependence of desorption and re-adsorption of the adsorbed molecules on a heated target surface, and the temperature required for proton-free carbon-ion acceleration can be estimated.

I. INTRODUCTION

Charged particles such as protons and heavy ions exhibit a characteristic curve of energy deposition vs depth, with a so-called Bragg peak, which enables the deposition of high radiation doses to tumors while reducing the dose to adjacent normal tissues.[1] Unlike protons, heavy ions deposit a small portion of their energy distally from the Bragg peak owing to nuclear fragmentation. Therefore, the ions used for radiotherapy are limited to species that are not heavier than oxygen. In 1994, the National Institute of Radiological Sciences (NIRS) commenced the first clinical trials of heavy-ion radiotherapy using carbon ions at the HIMAC facility. Carbon ions exhibit higher linear energy transfer (LET) than high-energy photons and protons, and a high LET induces sufficient damage to clustered DNA that cellular repair systems can be overwhelmed.[2] The benefit of using carbon-ion radiotherapy has been recognized by health authorities in several countries, leading to health insurance coverage of this treatment for several types of cancer.[3] Typical examples of such insurance coverage in Japan include high- and intermediate-risk prostate cancer, chordomas, chondrosarcomas, osteosarcomas, and salivary gland tumors, while tumor re-irradiation is also covered in Italy, Germany, and Austria.[4]

However, although carbon-ion cancer therapy is envisioned to bring significant benefits to patients, its availability is still very limited worldwide. The main reasons for this lack of widespread adoption are the high construction, installation, and routine maintenance costs of the complex and large accelerators that are required.[5]

The National Institutes for Quantum Science and Technology (QST) in Japan have progressed toward developing a compact accelerator for carbon-ion radiotherapy called "Quantum Scalpel" to overcome these issues.[3,6] The Quantum Scalpel consists of a laser-driven injector with an acceleration 4 MeV/u, a superconducting synchrotron of diameter 8 m, and a superconducting gantry. The required ion-beam parameters of the laser-driven ion injector were set with reference to the current ion injector at HIMAC using Radio frequency acceleration. The laser-driven ion injector needs to inject $>10^9$ carbon ions (C^{4+} or C^{6+}) with quasi-monochromatic energy (10% bandwidth) of 4 MeV per nucleon within 2 s. To suppress the beam divergence caused by space-charge effects during acceleration in the synchrotron, the maximum number of particles that can be injected in a single acceleration phase is limited to $\sim 10^8$. Therefore, 10^8 ions are repeatedly injected at 10 Hz until the required number of particles have been injected into the synchrotron. In addition, pre-accelerated ions are injected into the synchrotron after compression to 1% bandwidth using a phase rotation cavity. The synchrotron accelerates the carbon ions to 430 MeV/u, which is sufficient for heavy-ion radiotherapy. The gantry enables the treatment of tumors located deep inside the body from any direction.[7]

A laser-driven carbon-ion injector requires three systems (laser, target supply, and surface contamination cleaner) capable of operating at repetition rates over 10 Hz. With the recent advent of diode-pumped solid-state lasers,[8,9] it has become possible to irradiate with 10 J-class laser pulses at several Hz, and high-repetition-rate laser irradiation above 10 Hz is in sight.

With regard to the target, a single-layer thin film of high-purity carbon is very fragile and therefore difficult to supply at high repetition rate. We therefore plan to use a double-layer thin film, consisting of a thicker support metal film with a high-purity thin carbon layer. The carbon source layer must be resistant to high temperatures to prevent thermal desorption during contaminant cleaning. The solid solution of carbides or precipitated carbon that results from the catalytic effect of heating transition metals is a potential candidate for the carbon source layer owing to its high heat resistance.[10,11] In this study, we heated a tape of nickel, which is a transition metal, and formed a carbon layer originating from the contamination. This provided a thin carbon-rich layer for acceleration. As far as the target supply system is concerned, the conventional scheme of a motor driving a tape-shaped[12,13] or disk-shaped[14] solid target is scalable toward a high repetition rate.

However, the performance of surface contaminant cleaners is insufficient for the immediate cleaning of target surface contamination supplies at high repetition rates.[15] In the target normal sheath acceleration mechanism,[16,17] protons are selectively accelerated over other heavier ion species because they have the largest charge-to-mass ratio. The origin of these protons is known to be water vapor and hydrocarbons that adsorb to the target surface during the target manufacturing process or after installation in the vacuum chamber.[18] The surface contamination layer is about 1 nm thick[18,19] and comprises CH_2 (60%) and H_2O (12%).[19] The contaminant molecules are chemisorbed on the surface and require about 100 kJ/mol of energy for desorption.[18] Desorption of these molecules by thermal motion requires heating above 200 °C.[20]

A variety of contaminant cleaning techniques have been proposed, including blowing off surface contamination (pulsed laser ablation[21] and ion sputtering[19]) and heating the target (resistive heating[22] and continuous-wave laser heating[23,24]). However, the blow-off method generates unwanted target gas and debris that stress the vacuum system and laser focusing optics. These problems become more severe in highly repetitive operations. On the other hand, the heating methods reported so far do not provide sufficient heating power for immediate cleaning of the target surface supplied at high repetition rates (>10 Hz). Here, we report a new method of cleaning surface contamination by induction heating. The developed induction heater heats a 5-μm-thick nickel tape to over 400 °C in 100 ms and can be scaled to carbon-ion acceleration at 10 Hz in the near future.

II. INDUCTION HEATING FOR DESORPTION OF SURFACE CONTAMINATION

The induction heater consists of a coil and an electronic oscillator with a high-frequency alternating current (AC). When an AC is applied to a coil, a time-varying magnetic field is generated around the coil. When a conductor is placed near the coil, eddy currents I flow through the conductor to prevent changes in the magnetic field. Since the conductor has electrical resistance R, Joule heat corresponding to $I^2 \times R$ is generated, and the conductor is heated. The final process of induction heating is similar to resistive heating,[22] in which current is passed directly from electrodes attached to the target, but with three significant modifications.[25]

The first modification is that eddy currents are induced contactlessly by electromagnetic induction. Unlike resistive heating, there is no need to attach an electrode to each target, and thus this method is effective for applications that require the heating of objects that need to be replaced at a high repetition rate. The second modification is that eddy currents have the same frequency as the AC flowing in the coil, and so the eddy current flow is restricted to a thin layer of the conductor surface by the skin effect, greatly enhancing the heating effect. Nickel, a ferromagnetic material, is chosen as the target material. Because the high permeability of ferromagnetic materials increases the induced eddy currents and surface skin effect, magnetic materials are more easily heated by induction than nonmagnetic materials. Also, nickel is a transition metal, and at high temperatures it assists in the dehydrogenation of hydrocarbons through its catalytic effect.[10,11] In this study, carbon ions in a solid solution of carbides and precipitated carbon on heated nickel tapes were accelerated.

The magnetic material is heated by hysteresis losses, which is a minor benefit in this system. The third modification is that the shape of the coil can influence the shape of the eddy currents. We designed three concentrical turned coils (pancake-shaped) of copper pipe. Cooling water flowed inside the pipe, and AC flowed through the conductor portion of the pipe. The coils were placed 4 mm apart parallel to the tape target. The outer dimension of the coil was 25 mm, larger than the 20 mm width of the nickel tape [shown in Fig. 1(a)], i.e., both ends of the coil protruded from the tape. The temperature distribution of the heated nickel foil results

from the complex physical processes of induction heating. A finite element analysis code (Femtet ver. 2021[26]) was used to analyze the heating process. The temperature dependence of the physical properties of nickel (electrical resistivity,[27] thermal conductivity,[28] and specific permeability[29]) in the temperature range from room temperature to 1000 °C was considered in the simulation. Then, in the simulation, 25 A of AC was applied to the coil at a frequency of 400 kHz to ensure consistency with the experimental conditions.

The vector map in Fig. 1(b) shows the magnetic flux flow inside the nickel foil. Loop currents flowing in concentric coils produce a magnetic flux flow similar to that of a dipole magnet. If a ferromagnetic nickel foil is present to obstruct the magnetic flux flow, the magnetic flux will preferentially flow through the nickel rather than into the vacuum, resulting in a higher magnetic flux density with a thin nickel foil. As a result, the magnetic flux flows and accumulates in the center of the coil. This vector map of the magnetic field is a cutout of a particular time, and the magnetic field's direction and intensity change with the phase of the AC flowing through the coil.

The vector map in Fig. 1(c) shows the eddy current flow inside the nickel foil. The eddy current flows in the opposite direction on the same shape as the AC in the coil (in this case, a circle), and the induced magnetic field cancels the magnetic field created by the coil. Thus, the current density of eddy currents increases on the left and right sides of the circle region, where eddy currents flow, owing to the width limitation of the tape (coil diameter > tape width). This current density bias is vital to explain the hot-spot formation. The color map in Fig. 1(d) displays the temperature distribution of the heated nickel tape at 500 ms after heating was initiated. The temperature distribution obtained in the simulation had two semicircular hot spots.

Figure 2(a) shows the temperature distribution of the nickel tape experimentally observed by infrared thermography when the tape was heated at an AC power of 0.6 kW. The white dashed lines represent both ends of the 20-mm-wide tape, and the black dashed lines indicate the simulated 350 °C isotherm. The temperature distribution observed experimentally accurately reproduces the distribution obtained in the simulation, including the asymmetry of the hotspot due to the coil asymmetry. The red line in Fig. 2(b) depicts the time variation of the temperature of the left hotspot [the small white square region in Fig. 2(a)] during heating. A partial volume of nickel tape (~5 mm × 5 mm × 5 μm) was heated to 400 °C in ~100 ms. From the specific heat of nickel and the volume of the heating area, the heating areal power density due to induction heating is estimated to be about 2 W/cm^2. When the target is heated to about 400 °C, about 2 W/cm^2 of energy is lost by radiation. Radiation loss and heat generation are balanced, and the temperature rise saturates.

The target temperature under laser irradiation varies with the time interval between heating and irradiation. The blue line in Fig. 2(c) depicts the time variation of the hot-spot temperature after removal from the heating coil. When the vacuum pressure is 0.05 Pa, the vacuum gap limits thermal conduction along the perpendicular direction to the nickel surface. The nickel tape heated up to 400 °C cooled rapidly to 180 °C within 1 s (radiation cooling); it then cooled slowly to below 100 °C for about 12 s (thermal conduction).

III. LASER-DRIVEN CARBON-ION ACCELERATION

We used laser-driven ion acceleration as a time-resolved analytical technique for surface contamination, and the temperature dependence of the desorption and readsorption of the adsorbate molecules was evaluated. A linearly polarized (p-polarized on target), 40 fs laser pulse (FWHM) with a central wavelength of 795 nm was focused on a 5-μm-thick nickel foil at a 45° incidence angle using an F/2.7 off-axis parabolic mirror. Then, 23% of the total energy of 389 mJ was focused into a focal spot with a diameter of 5 μm (FWHM), and the average laser intensity in the spot was $(6 \pm 1) \times 10^{18}$ W/cm^2.

The top spool was pre-wound with nickel tape, and a motor-driven rubber roller (composed of heat-resistant silicon that can be used for 10 000 h or more at 200 °C) drew the tape target from the top spool. The heating coil was placed 10 cm along the tape pass above the laser irradiation point (Fig. 3).

A series of experiments were performed under the six conditions depicted in Fig. 4: a no-heating condition and five cases of heating conditions with varying target temperatures under laser irradiation (50, 80, 110, 130 and 150 °C). The target temperature at the laser irradiation point was varied with the time interval between heating and laser irradiation. Accelerated ion species were analyzed using a Thomson parabola ion spectrometer.[30] Ions were detected by a phosphor screen and the scintillation light was transported using a lens and recorded by a cooled charged-coupled device camera. The strongest trace agrees with that of the theoretical trace of the proton (i.e., Z/A = 1.00) in Fig. 4(a) under the no-heating condition. The charge-to-mass ratios Z/A of the weaker four traces observed in Fig. 4(a) are estimated to be 0.083, 0.17, 0.25, and 0.33. These ratios are consistent with the theoretical charge-to-mass ratios of C^+, C^{2+}, C^{3+}, and C^{4+}, respectively.

Under the five heating conditions (50, 80, 110, 130, and 150 °C), ion species with different trends were accelerated. When the target temperature cooled to 50 °C and to 80 °C, the proton signal was dominant, as in the nonheated case, and the maximum charge state of the carbon ions was 4 [Figs. 4(b) and 4(c)]. These results indicate that once desorbed by heating, hydrogen was reabsorbed by the surface as it cooled below 80 °C. In the cases of 110 and 130 °C [Figs. 4(d) and 4(e)], the proton signal was still dominantly observed, but the maximum charge state of the carbon ions increased to 5, and the signal of higher-energy carbon ions was increased. Nickel ions originating from the target bulk were also accelerated. When the laser was promptly irradiated and kept at 150 °C [Fig. 4(f)], the proton signal was reduced, and the C^{4+} and C^{5+} ion signals were dominant.

An analysis code can be used to precisely link the particle position on the detector with its kinetic energy and convert the recorded parabolic traces into ion spectra. The ion spectra under the no-heating condition [Fig. 4(a)] are illustrated in Fig. 4(h). The ion spectra were corrected by subtracting the background signals generated by the high-energy x-rays and the scattered ions from the pinhole. The maximum energies of protons and carbon ions were observed to be 1.0 MeV (H^+) and 0.9 MeV (C^{1+}), 1.3 MeV (C^{2+}), 2.05 MeV (C^{3+}), and 2.5 MeV (C^{4+}). Figure 4(i) depicts the ion spectra for the heating condition at 150 °C [Fig. 4(f)]. The maximum energies of protons and carbon ions were observed to be 1.0 MeV (H^+) and 3.25 MeV (C^{3+}), 5.2 MeV (C^{4+}), and 6.52 MeV (C^{5+}).

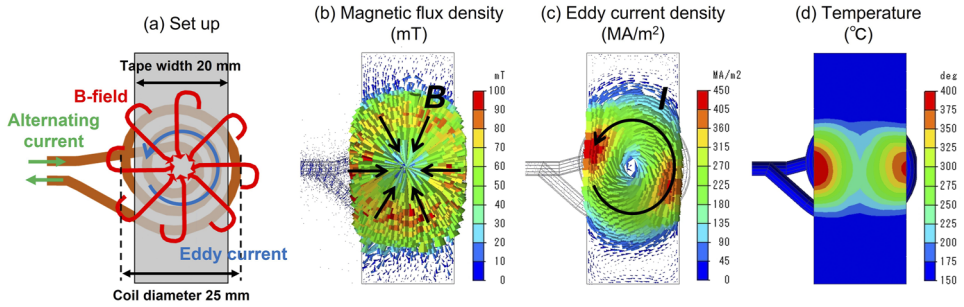

FIG. 1. A finite element analysis code (Femtet ver. 2021) was used to analyze the heating process. (a) Schematic view of setup. (b) Magnetic flux flow inside the nickel foil. (c) Eddy current flow inside the nickel foil. (d) Temperature distribution of the heated nickel tape.

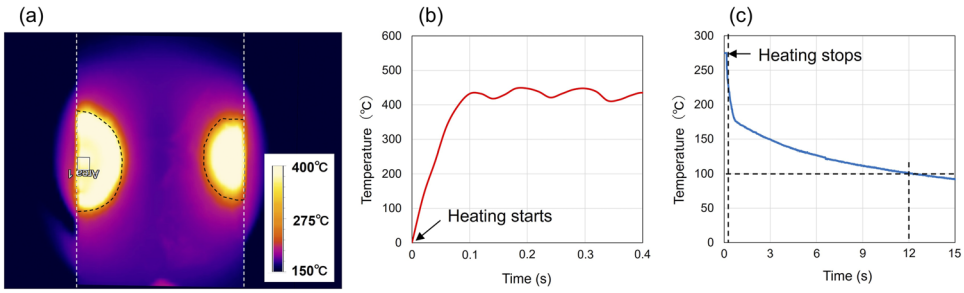

FIG. 2. (a) Temperature distribution of the nickel tape observed by infrared thermography when heated at an AC power of 0.6 kW. (b) Time variation of the temperature of the hotspot during heating. (c) Time variation of the hot-spot temperature after removal from the heating coil.

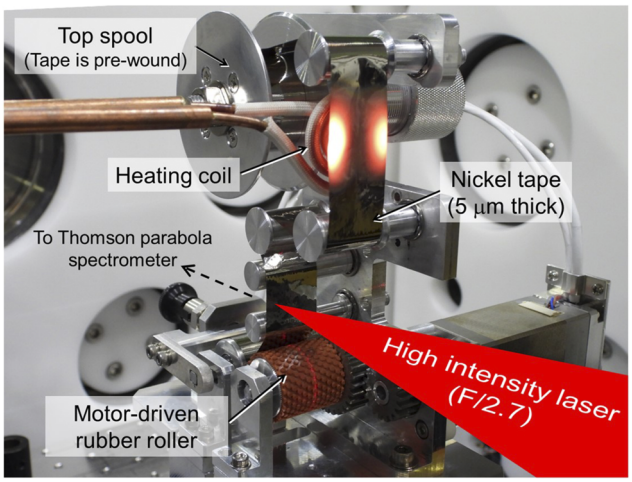

FIG. 3. Experimental setup for the demonstration of laser-driven carbon-ion acceleration using an induction heater.

Regardless of the difference in the conditions with no heating [Fig. 4(h)] and heating [Fig. 4(i)], the maximum proton energy remained constant at 1 MeV. However, the number of protons in the low-energy region (<0.5 MeV) decreased by two orders of magnitude. Moreover, in the energy spectra of the carbon ions, the maximum charge state of the accelerated carbon ions increased from 4 to 5, with the maximum energy increasing to 6.5 MeV. These results indicate that heating caused the desorption of contaminant hydrogen and reduced the coverage of the contamination layer such that the sheath field for TNSA could efficiently accelerate the carbon ions.

IV. ADSORBED MOLECULES ON A HEATED TARGET SURFACE

The difference in behavior between the accelerated ion species can be explained by the Langmuir adsorption model, which gives the equilibrium coverage of molecules on a solid surface. Whenever gas (adsorbate) is in contact with a solid surface (adsorbent), an equilibrium will be established between the adsorption rate of molecules on the surface and the desorption rate of molecules to the gas phase. The equilibrium coverage of molecules on a solid surface is given by

$$\theta = \frac{p}{p + p_0(T)},$$

where

$$p_0(T) = \left(\frac{2\pi m k_B T}{h^2}\right)^{3/2} k_B T \exp\left(-\frac{\varepsilon / N_A}{k_B T}\right).$$

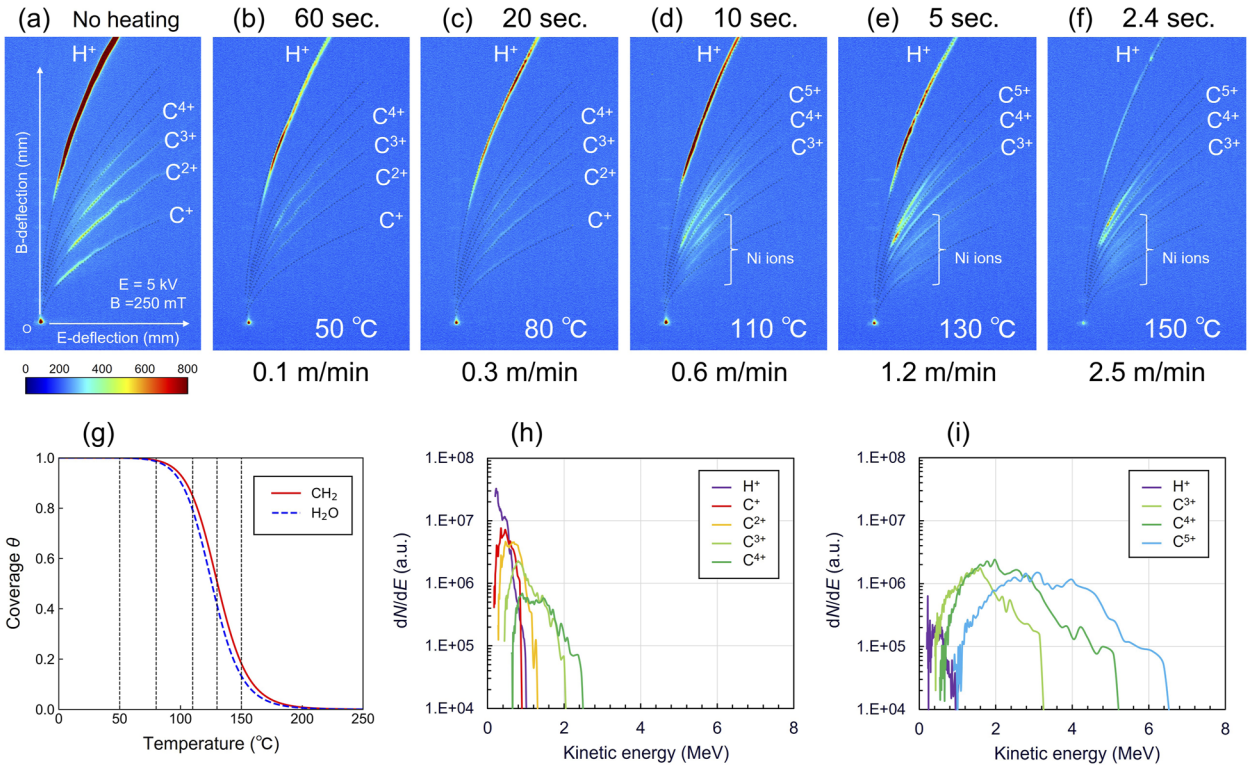

FIG. 4. Traces from the Thomson parabola spectometer observed under six experimental conditions: a no-heating condition (a) and five heating conditions, namely, 50 °C (b), 80 °C (c), 110 °C (d), 130 °C (e), and 150 °C (f). (g) Equilibrium coverage calculated from the Langmuir adsorption model. (h) Ion spectra for the no-heating condition. (i) Ion spectra for the 150 °C heating condition.

Here, k_B, h, N_A, and T are Boltzmann's constant, Planck's constant, Avogadro's constant, and the temperature of the adsorbent, respectively. m, p, and ε are the adsorbate's mass, partial pressure, and activation energy, respectively. Figure 4(g) shows the isobar (p = 0.05 Pa) calculated from the Langmuir adsorption model. CH_2 (red solid line) or H_2O (blue dotted line) were assumed as adsorbate molecules.

For both molecules, the equilibrium coverage is expected to be nearly zero at temperatures above 200 °C, exposing the nickel bulk. Coverage increases as the nickel tape cools, with the bulk nickel surface completely covered by a single contaminating molecular layer at around 80 °C. Experimental data show that both protons from contamination and nickel ions from the bulk were accelerated at 110 °C, but the nickel ion signal disappeared at 80 °C. The Langmuir adsorption model accurately explained the experimentally observed differences in ion species with respect to temperature. Therefore, if the nickel is kept above 200 °C until the laser irradiation, heavy ions are expected to be accelerated under proton-free conditions. However, high-temperature nickel is known to have a high affinity for carbon, drawing carbon from hydrocarbons and forming solid solutions of carbides and carbon on the surface and inside the bulk. Therefore, it is essential to note that heating nickel above 200 °C does not cause acceleration of pure nickel. However, this property is useful for application to current heavy-ion accelerators for cancer therapy that use carbon ions.

V. CONCLUSION

The induction heating contamination cleaner reported here is a practical method for laser-driven heavy-ion acceleration at high repetition rates because it is debris-free, unlike the blow-off method, and has high heating power, unlike conventional heating methods. Additionally, induction heating can heat any conductive material, and cleaning the contamination layer can accelerate the bulk ions. Therefore, this cleaning method can be applied to acceleration of heavy ions produced from conductive materials with a wide range of atomic numbers. In particular, the noncontact property of induction heating is effective for heating fragile, ultrathin targets (with a thickness of tens to hundreds of nanometers), which are used for radiation pressure acceleration. As the conversion efficiency decreases from high-frequency magnetic field to eddy currents for thinner targets, the target volume is reduced as well, which is expected to maintain a high heating performance up to higher temperatures.

Even insulators and room-temperature gaseous atoms can be accelerated by constructing a multilayer structure with a conductor layer. For example, gaseous molecules such as helium, argon, oxygen, and neon can be pre-embedded on the surface of a thin conductor film using a sputter gun.[31] Current heavy-ion cancer therapy is performed using carbon ions, but heavier ions, such as oxygen and neon, may be more effective in treating difficult-to-treat cancers, such as pancreatic cancer. Conversely, for cancers

that respond well to radiotherapy, the use of lighter ions, such as helium, for treatment causes less damage to the tissues surrounding the cancer. Therefore, a multi-ion species therapy using helium, carbon, oxygen, and neon has been proposed, depending on the nature of the tumor and the surrounding environment.[7] The cleaning method described in this paper has great potential for future application in heavy-ion cancer therapy. We envision this type of contamination cleaner to form the basis of a laser-driven heavy-ion accelerator, such as the "Quantum Scalpel."[32] Such a laser-driven heavy-ion accelerator will reduce the facility size and construction cost of heavy-ion cancer therapy devices and enable their widespread use.

ACKNOWLEDGMENTS

This work was supported by the Japanese Ministry of Education, Culture, Sports, Science and Technology (MEXT) through the JST-Mirai Program (Grant No. JPMJMI17A1) and Grants-in-Aid, KAKENHI (Grant Nos. 21J22132 and 22K14021).

AUTHOR DECLARATIONS

Conflict of Interest

The authors have no conflicts to disclose.

Author Contributions

Sadaoki Kojima: Formal analysis (lead); Software (lead); Visualization (lead); Writing – original draft (lead). **Tatsuhiko Miyatake**: Methodology (equal); Resources (equal); Writing – review & editing (equal). **Hironao Sakaki**: Project administration (equal); Writing – review & editing (equal). **Hiroyoshi Kuroki**: Conceptualization (equal); Methodology (equal); Resources (equal). **Yusuke Shimizu**: Conceptualization (equal); Methodology (equal); Resources (equal). **Hisanori Harada**: Conceptualization (equal); Methodology (equal); Resources (equal). **Norihiro Inoue**: Conceptualization (equal); Methodology (equal); Resources (equal). **Thanh Hung Dinh**: Methodology (equal); Resources (equal); Writing – review & editing (equal). **Masayasu Hata**: Writing – review & editing (equal). **Noboru Hasegawa**: Writing – review & editing (equal). **Michiaki Mori**: Writing – review & editing (equal). **Masahiko Ishino**: Writing – review & editing (equal). **Mamiko Nishiuchi**: Writing – review & editing (equal). **Kotaro Kondo**: Writing – review & editing (equal). **Masaharu Nishikino**: Supervision (equal); Writing – review & editing (equal). **Masaki Kando**: Supervision (equal); Writing – review & editing (equal). **Toshiyuki Shirai**: Funding acquisition (equal); Supervision (equal); Writing – review & editing (equal). **Kiminori Kondo**: Funding acquisition (equal); Project administration (equal); Supervision (equal); Writing – review & editing (equal).

DATA AVAILABILITY

The data that support the findings of this study are available from the corresponding author upon reasonable request.

REFERENCES

[1]K. Ledingham, P. Bolton, N. Shikazono, and C.-M. Ma, "Towards laser driven hadron cancer radiotherapy," Appl. Sci. **4**, 402 (2014).
[2]T. D. Malouff, A. Mahajan, S. Krishnan, C. Beltran, D. S. Seneviratne, and D. M. Trifiletti, "Carbon ion therapy: A modern review of an emerging technology," Front. Oncol. **10**, 82 (2020).
[3]H. Ishikawa, Y. Hiroshima, N. Kanematsu, T. Inaniwa, T. Shirai, R. Imai, H. Suzuki, K. Akakura, M. Wakatsuki, T. Ichikawa, and H. Tsuji, "Carbon-ion radiotherapy for urological cancers," Int. J. Urol. **29**, 1109 (2022).
[4]A. Pompos, R. L. Foote, A. C. Koong, Q. T. Le, R. Mohan, H. Paganetti, and H. Choy, "National effort to re-establish heavy ion cancer therapy in the United States," Front. Oncol. **12**, 880712 (2022).
[5]U. Amaldi, R. Bonomi, S. Braccini, M. Crescenti, A. Degiovanni, M. Garlasché, A. Garonna, G. Magrin, C. Mellace, P. Pearce, G. Pittà, P. Puggioni, E. Rosso, S. Verdú Andrés, R. Wegner, M. Weiss, and R. Zennaro, "Accelerators for hadrontherapy: From Lawrence cyclotrons to linacs," Nucl. Instrum. Methods Phys. Res., Sect. A **620**, 563 (2010).
[6]N. Kanematsu, T. Furukawa, Y. Hara, T. Inaniwa, Y. Iwata, K. Mizushima, S. Mori, and T. Shirai, "New technologies for carbon-ion radiotherapy—Developments at the National Institute of Radiological Sciences, QST, Japan," Radiat. Phys. Chem. **162**, 90 (2019).
[7]Y. Iwata, T. Shirai, K. Mizushima, S. Matsuba, Y. Yang, E. Noda, M. Urata, M. Muramatsu, K. Katagiri, S. Yonai, T. Inaniwa, S. Sato, Y. Abe, T. Fujimoto, T. Sasano, T. Shiraishi, T. Suzuki, K. Takahashi, K. Kondo, H. Sakaki, M. Nishiuchi, T. Orikasa, S. Takayama, S. Amano, K. Nakanishi, M. Tachibana, Y. Touchi, S. Tsubomatsu, and S. Nomura, "Design of a compact superconducting accelerator for advanced heavy-ion therapy," Nucl. Instrum. Methods Phys. Res., Sect. A **1053**, 168312 (2023).
[8]R. Lera, P. Bellido, I. Sanchez, P. Mur, M. Seimetz, J. M. Benlloch, M. Roso, L. Ruiz-de-la-Cruz, and A. Ruiz-De-La-Cruz, "Development of a few TW Ti:Sa laser system at 100 Hz for proton acceleration," Appl. Phys. B **125**, 4 (2019).
[9]S. Borneis, T. Laštovička, M. Sokol, T.-M. Jeong, F. Condamine, O. Renner, V. Tikhonchuk, H. Bohlin, A. Fajstavr, J.-C. Hernandez, N. Jourdain, D. Kumar, D. Modřanský, A. Pokorný, A. Wolf, S. Zhai, G. Korn, and S. Weber, "Design, installation and commissioning of the ELI-Beamlines high-power, high-repetition rate HAPLS laser beam transport system to P3," High Power Laser Sci. Eng. **9**, e30 (2021).
[10]X. Li, W. Cai, L. Colombo, and R. S. Ruoff, "Evolution of graphene growth on Ni and Cu by carbon isotope labeling," Nano Lett. **9**, 4268 (2009).
[11]B. M. Hegelich, B. J. Albright, J. Cobble, K. Flippo, S. Letzring, M. Paffett, H. Ruhl, J. Schreiber, R. K. Schulze, and J. C. Fernández, "Laser acceleration of quasi-monoenergetic MeV ion beams," Nature **439**, 441 (2006).
[12]M. Noaman-ul-Haq, H. Ahmed, T. Sokollik, L. Yu, Z. Liu, X. Yuan, F. Yuan, M. Mirzaie, X. Ge, L. Chen, and J. Zhang, "Statistical analysis of laser driven protons using a high-repetition-rate tape drive target system," Phys. Rev. Accel. Beams **20**, 041301 (2017).
[13]M. Nishikino, Y. Ochi, N. Hasegawa, T. Kawachi, H. Yamatani, T. Ohba, T. Kaihori, and K. Nagashima, "Demonstration of a highly coherent 13.9 nm x-ray laser from a silver tape target," Rev. Sci. Instrum. **80**, 116102 (2009).
[14]C. Ruiz, J. Benlliure, D. Cortina, D. González, J. Llerena, and L. Martín, "Development of a multi-shot experiment for proton acceleration," J. Phys.: Conf. Ser. **1079**, 012009 (2018).
[15]G. M. Petrov, L. Willingale, J. Davis, T. Petrova, A. Maksimchuk, and K. Krushelnick, "The impact of contaminants on laser-driven light ion acceleration," Phys. Plasmas **17**, 103111 (2010).
[16]P. Mora, "Plasma expansion into a vacuum," Phys. Rev. Lett. **90**, 185002 (2003).
[17]Y. Sentoku, T. E. Cowan, A. Kemp, and H. Ruhl, "High energy proton acceleration in interaction of short laser pulse with dense plasma target," Phys. Plasmas **10**, 2009 (2003).
[18]Z. Lécz, J. Budai, A. Andreev, and S. Ter-Avetisyan, "Thickness of natural contaminant layers on metal surfaces and its effects on laser-driven ion acceleration," Phys. Plasmas **27**, 013105 (2020).
[19]M. Allen, P. K. Patel, A. Mackinnon, D. Price, S. Wilks, and E. Morse, "Direct experimental evidence of back-surface ion acceleration from laser-irradiated gold foils," Phys. Rev. Lett. **93**, 265004 (2004).

[20]K. Fukutani, "Surfaces in vacuum technology," J. Vac. Soc. Jpn. **56**, 204 (2013).
[21]P. Sommer, J. Metzkes-Ng, F. E. Brack, T. E. Cowan, S. D. Kraft, L. Obst, M. Rehwald, H. P. Schlenvoigt, U. Schramm, and K. Zeil, "Laser-ablation-based ion source characterization and manipulation for laser-driven ion acceleration," Plasma Phys. Controlled Fusion **60**, 054002 (2018).
[22]M. Hegelich, S. Karsch, G. Pretzler, D. Habs, K. Witte, W. Guenther, M. Allen, A. Blazevic, J. Fuchs, J. C. Gauthier, M. Geissel, P. Audebert, T. Cowan, and M. Roth, "MeV ion jets from short-pulse-laser interaction with thin foils," Phys. Rev. Lett. **89**, 085002 (2002).
[23]D. T. Offermann, K. A. Flippo, S. A. Gaillard, D. C. Gautier, S. Letzring, J. C. Cobble, G. Wurden, R. P. Johnson, T. Shimada, D. S. Montgomery, R. P. Gonzales, T. Hurry, F. Archuleta, M. J. Schmitt, S. M. Reid, T. Bartal, M. S. Wei, D. P. Higginson, F. N. Beg, M. Geissel, and M. Schollmeier, "Carbon ion beam focusing using laser irradiated, heated diamond hemispherical shells," J. Phys.: Conf. Ser. **244**, 022053 (2010).
[24]K. Kondo, M. Nishiuchi, H. Sakaki, N. P. Dover, H. F. Lowe, T. Miyahara, Y. Watanabe, T. Ziegler, K. Zeil, U. Schramm, E. J. Ditter, G. S. Hicks, O. C. Ettlinger, Z. Najmudin, H. Kiriyama, M. Kando, and K. Kondo, "High-intensity laser-driven oxygen source from CW laser-heated titanium tape targets," Crystals **10**, 837 (2020).
[25]V. Rudnev, D. Loveless, and R. L. Cook, *Handbook of Induction Heating*, 2nd ed. (CRC Press, Routledge, 2017).
[26]FEMTET, Murata Software Co., Ltd., https://www.muratasoftware.com/en/ (2021).
[27]L. Abadlia, F. Gasser, K. Khalouk, M. Mayoufi, and J. G. Gasser, "New experimental methodology, setup and LabView program for accurate absolute thermoelectric power and electrical resistivity measurements between 25 and 1600 K: Application to pure copper, platinum, tungsten, and nickel at very high temperatures," Rev. Sci. Instrum. **85**, 095121 (2014).
[28]J. Yin, H. Zhu, L. Ke, P. Hu, C. He, H. Zhang, and X. Zeng, "A finite element model of thermal evolution in laser micro sintering," Int. J. Adv. Manuf. Technol. **83**, 1847 (2016).
[29]J. L. Glathart, "The inner, initial, magnetic permeability of iron and nickel at ultra-high radiofrequencies," Phys. Rev. **55**, 833 (1939).
[30]S. Kojima, S. Inoue, T. H. Dinh, N. Hasegawa, M. Mori, H. Sakaki, Y. Yamamoto, T. Sasaki, K. Shiokawa, K. Kondo, T. Yamanaka, M. Hashida, S. Sakabe, M. Nishikino, and K. Kondo, "Compact Thomson parabola spectrometer with variability of energy range and measurability of angular distribution for low-energy laser-driven accelerated ions," Rev. Sci. Instrum. **91**, 053305 (2020).
[31]J. Schreiber, M. Kaluza, F. Grüner, U. Schramm, B. M. Hegelich, J. Cobble, M. Geissler, E. Brambrink, J. Fuchs, P. Audebert, D. Habs, and K. Witte, "Source-size measurements and charge distributions of ions accelerated from thin foils irradiated by high-intensity laser pulses," Appl. Phys. B: Lasers Opt. **79**, 1041 (2004).
[32]K. Noda, "Progress of radiotherapy technology with HIMAC," J. Phys.: Conf. Ser. **1154**, 012019 (2019).